Manipulating Goldstone modes via superradiant light in a bosonic lattice gas inside a cavity

Huan Wang,[1] Shuai Li,[1] Maksims Arzamasovs,[1] W. Vincent Liu,[2,3] and Bo Liu[1,*]

[1]*MOE Key Laboratory for Nonequilibrium Synthesis and Modulation of Condensed Matter,Shaanxi Province Key Laboratory of Quantum Information and Quantum Optoelectronic Devices, School of Physics, Xi'an Jiaotong University, Xi'an 710049, China*

[2]*Department of Physics and Astronomy, University of Pittsburgh, Pittsburgh, Pennsylvania 15260, USA*

[3]*Department of Physics and Shenzhen Institute for Quantum Science and Engineering, Southern University of Science and Technology, Shenzhen 518055, China*

(Received 19 October 2021; revised 30 March 2022; accepted 16 May 2022; published 3 June 2022)

We study the low-energy excitations of a bosonic lattice gas with cavity-mediated interactions. By performing two successive Hubbard-Stratonovich transformations, we derive an effective field theory to study the strongly coupling regime. Taking into account the quantum fluctuation, we report the unusual effect of the superradiant cavity light-induced density imbalance, which has been shown to have a negligible effect on the low-energy excitation spectrum in previous studies. Instead, we show that such infinitesimal fluctuation of density imbalance dramatically changes the behavior of low-energy excitations and results in a parameter-driven switching between two types of Goldstone modes, i.e., type I and type II with odd and even power energy-momentum dispersion, respectively. Our proposal would open a horizon for manipulating Goldstone modes by bridging the cavity light and strongly interacting quantum matters.

DOI: 10.1103/PhysRevA.105.063301

I. INTRODUCTION

The mechanism of spontaneous symmetry breaking is crucial for understanding phase transitions and is also widely used to study the associated emergence of new particles and excitations [1]. It is well known that when a continuous symmetry is spontaneously broken in nonrelativistic theories, there appear Nambu-Goldstone (NG) modes [2,3], the dispersion relations of which are either linear (type I) or quadratic (type II), where the numbers of distinct types of NG modes satisfy the Nielsen-Chadha inequality [4]. Thanks to recent experimental developments, the Goldstone modes have been studied in various condensed matter [5–8] and ultracold atomic systems [9–16].

A gas of bosonic atoms in an optical lattice has been reversibly tuned between superfluids (SF) and insulating ground states by varying the strength of the periodic potential [17,18]. It provides an ideal platform to study the spontaneous symmetry breaking induced elementary excitations. Not only has the gapless Goldstone mode been found to exhaust all of the spectral weight in the weakly interacting limit, but also the Higgs amplitude mode has been detected in the strongly interacting regime near the transition between SF and Mott state at commensurate fillings [19–21].

Recently, a complimentary approach using ultracold atoms inside a cavity unveiled the effect of cavity-mediated interactions, which resulted in the observation of a rich phase diagram with Mott insulator (MI), superfluid, supersolid (SS), and charge-density-wave (CDW) phases [22,23]. The low-energy excitations associated with the above various symmetry-breaking phases have been investigated within the framework of the mean-field approach, where new features, such as the softening of particle- and holelike excitations, have been explored [24]. The quantum fluctuation has not been taken into account within such mean-field calculations. However, it has been shown to play an important role in the strongly interacting regime, leading to intriguing physical phenomena, such as the appearance of the Higgs mode in the excitation spectrum of the Bose-Hubbard model [25,26].

In this work, we have developed an extension of the strong-coupling expansion technique for the system of ultracold bosons in an optical lattice strongly coupled to a single mode of a high-finesse optical cavity [22,23]. Such a strong-coupling expansion method has been successfully applied to describe various bosonic lattice gas systems, including the early studies of single-component bosonic lattice gases [27–30], systems incorporating the presence of a synthetic gauge field [31–35], and the degenerated p-orbitals [36]. Many interesting properties of these systems, such as the MI-SF phase transition, the excitation spectrum, etc., have been properly captured [27–36]. By employing such a well-developed method, the effect of quantum fluctuations in our proposed system can thus be systematically explored in the strongly interacting regime, which has not been studied previously [24,37]. Interestingly, we find that the quantum fluctuations at the SS-to-CDW transition cause an unexpected effect of the modulation of density imbalance, neglected in the previous studies [24]. While small, this modulation results in dramatic changes of the behavior of low-energy collective excitations. A parameter-driven switching between odd (type I) and even (type II) power energy-momentum dispersion NG modes can be achieved along the phase boundary. This

*liubophy@gmail.com

prediction would pave the way to manipulate NG modes in a cold-atom-based system.

II. EFFECTIVE MODEL

As with the ETH (Swiss Federal Institute of Technology in Zurich) experiment [22], here we consider a Bose-Einstein condensate (BEC), such as ^{87}Rb atoms, subjected to an ultrahigh-finesse optical cavity, where three mutually orthogonal standing waves form a highly anisotropic three-dimensional (3D) optical lattice $V_L(\mathbf{r}) = V_y \cos^2(q_0 y) + V_{2D}[\cos^2(q_0 x) + \cos^2(q_0 z)]$ with the lattice depth $V_y \gg V_{2D}$ and the wave vectors of laser fields denoted by q_0. The BEC is thus split into a stack of 2D layers, where the bosonic atoms are exposed to an additional potential $V_c(\mathbf{r}) = \hbar\bar{\eta}(\hat{a} + \hat{a}^\dagger)\cos(q_0 x)\cos(q_0 z) - \hbar(\Delta_c - U_0\cos^2(q_0 z))\hat{a}\hat{a}^\dagger$ in the xz-plane formed by the coherent scattering between one free-space lattice and one intracavity optical standing wave with the same wave vector q_0 [22,23]. $\bar{\eta}$ is the two-photon Rabi frequency determining the scattering rate. $\hat{a}$ and $\hat{a}^\dagger$ are the annihilation and creation operators for the cavity photon, respectively. $\Delta_c = \omega_p - \omega_c$ describes the discrepancy between pumping light (lattice standing-wave) frequency ω_p and the cavity resonance frequency ω_c. U_0 captures the maximum light shift per atom resulting from the effect of the dispersive shift of the cavity resonance frequency [22].

Since the coherent scattering of light between the lattice and the cavity mode creates a dynamical checkerboard superlattice for the atoms, the effective Hamiltonian describing the atomic dynamics dressed by the cavity field can be expressed as

$$H = \sum_{\mathbf{r},\mathbf{r}'} -T_{\sigma\sigma'}(\mathbf{r}-\mathbf{r}')\psi^\dagger_\sigma(\mathbf{r})\psi_{\sigma'}(\mathbf{r}') - \sum_{\mathbf{r},\sigma}\mu_\sigma n_\sigma(\mathbf{r}) + \frac{U}{2}\sum_{\mathbf{r},\sigma} n_\sigma(\mathbf{r})[n_\sigma(\mathbf{r})-1] - \delta_c|\alpha|^2, \tag{1}$$

where $\psi_\sigma(\mathbf{r})$ is the bosonic atom field. $\sigma = e, o$ stands for even and odd sites, respectively, describing distinct sublattices of the checkerboard lattice. Here we choose the nearest-neighbor two sites as one unit cell, and $\mathbf{r}$ ($\mathbf{r}'$) is the lattice index capturing the location of the unit cell. The expression of the hopping matrix $T_{\sigma\sigma'}$ is given in Appendix A. U captures the strength of the repulsive interaction between bosonic atoms determined by the effective s-wave scattering length, which can be tuned by means of the Feshbach resonance and lattice depth. $n_\sigma(\mathbf{r}) = \psi^\dagger_\sigma(\mathbf{r})\psi_\sigma(\mathbf{r})$ is the density operator. The on-site energies $\mu_e = \mu - \eta(\alpha^* + \alpha)$ and $\mu_o = \mu + \eta(\alpha^* + \alpha)$ are introduced for even and odd sites, respectively, where μ is the chemical potential and η is the energy shift due to the two-photon Rabi process. $\delta_c = \hbar(\Delta_c - \delta)$ is the energy detuning between the cavity and the pumping lights, where δ is the dispersive shift of the cavity due to the BEC [22]. α is the mean value of the cavity field, which can be determined by the steady equation $i\hbar\partial_t\alpha = \langle[\hat{a}, \tilde{\mathbf{H}}]\rangle - i\kappa\alpha = 0$ with $\tilde{\mathbf{H}} = -\sum_{\mathbf{r},\mathbf{r}'} T_{\sigma\sigma'}(\mathbf{r}-\mathbf{r}')\psi^\dagger_\sigma(\mathbf{r})\psi_{\sigma'}(\mathbf{r}') - \mu\sum_{\mathbf{r},\sigma} n_\sigma(\mathbf{r}) + \frac{U}{2}\sum_{\mathbf{r},\sigma} n_\sigma(\mathbf{r})[n_\sigma(\mathbf{r}) - 1] + \eta(\hat{a} + \hat{a}^\dagger)\sum_{\mathbf{r}}[n_e(\mathbf{r}) - n_o(\mathbf{r})] - \hbar(\Delta_c - \delta)\hat{a}^\dagger\hat{a}$ in the regime of large decay rate κ [38], and it leads to the following relation:

$$\alpha = \frac{\eta\sum_{\mathbf{r}}[\langle n_e(\mathbf{r})\rangle - \langle n_o(\mathbf{r})\rangle]}{\delta_c + i\kappa} \overset{|\Delta_c|\gg\kappa,|\delta|}{\approx} \frac{N\eta(\langle n_e\rangle - \langle n_o\rangle)}{\hbar\Delta_c}, \tag{2}$$

where $\langle n_e(\mathbf{r})\rangle$ and $\langle n_o(\mathbf{r})\rangle$ are the average density of bosonic atoms at even and odd sites, respectively. $2N$ is the total lattice site.

III. PATH INTEGRAL APPROACH

In the following, we apply the strong-coupling expansion to the model Hamiltonian in Eq. (1), which extends the treatment in the Bose-Hubbard model [27], where both superfluid and Mott phases can be captured at the same time by this method. Through introducing the complex field ψ_σ, the thermodynamic properties of the system can be obtained from the partition function Z as a functional integral with the action $S[\psi^*_\sigma, \psi_\sigma] = \int_0^\beta d\tau\{\sum_{\sigma,\mathbf{r}}\psi^*_\sigma(\mathbf{r})\partial_\tau\psi_\sigma(\mathbf{r}) + H[\psi^*, \psi]\}$. Here, τ is an imaginary time and $\beta = 1/k_B T$ is the inverse temperature. We then perform a Hubbard-Stratonovich transformation through introducing the auxiliary field ϕ_σ to decouple the intersite hopping in the action, and we obtain

$$\begin{aligned}
Z &= \int D[\psi^*_\sigma, \psi_\sigma, \phi^*_\sigma, \phi_\sigma] \\
&\quad\times \exp\left\{-\int_0^\beta d\tau \sum_{\mathbf{r},\mathbf{r}'}\phi^*_\sigma(\mathbf{r})T^{-1}_{\sigma\sigma'}\phi_{\sigma'}(\mathbf{r}') \right. \\
&\quad\left. + \left[\sum_{\sigma,\mathbf{r}}\int_0^\beta d\tau\phi^*_\sigma(\mathbf{r})\psi_\sigma(\mathbf{r}) + \text{c.c.}\right] - S_0[\psi^*_\sigma, \psi_\sigma]\right\} \\
&= Z_0\int D[\phi^*_\sigma, \phi_\sigma]e^{-\int_0^\beta d\tau\sum_{\mathbf{r},\mathbf{r}'}\phi^*_\sigma(\mathbf{r})T^{-1}_{\sigma\sigma'}\phi_{\sigma'}(\mathbf{r}')} \\
&\quad\times\left\langle\exp\left[\sum_{\sigma,\mathbf{r}}\int_0^\beta d\tau\phi^*_\sigma(\mathbf{r})\psi_\sigma(\mathbf{r}) + \text{c.c.}\right]\right\rangle_0 \\
&= Z_0\int D[\phi^*_\sigma, \phi_\sigma] \\
&\quad\times\exp\left\{-\int_0^\beta d\tau\sum_{\mathbf{r},\mathbf{r}'}\phi^*_\sigma T^{-1}_{\sigma\sigma'}\phi_{\sigma'} + W[\phi^*_\sigma, \phi_\sigma]\right\},
\end{aligned} \tag{3}$$

where $T^{-1}_{\sigma\sigma'}$ represents the inverse hopping matrix. S_0 and Z_0 are the action and partition function in the limit of $t = 0$. $\langle\cdots\rangle_0$ stands for averaging with S_0. $W[\phi^*_\sigma, \phi_\sigma] = \ln\langle\exp[\sum_{\sigma,\mathbf{r}}\int_0^\beta d\tau\phi^*_\sigma(\mathbf{r})\psi_\sigma(\mathbf{r}) + \text{c.c.}]\rangle_0$ is the generation function linking to connected local Green's functions G^{Rc} through the relation [25] $W[\phi^*, \phi] = \sum_{R=1}^\infty\frac{(-1)^R}{(R!)^2}\sum'_{\sigma_1\cdots\sigma'_R}G^{Rc}_{\{\sigma_i,\sigma'_i\}}\phi^*_{\sigma_1}\cdots\phi^*_{\sigma_R}\phi_{\sigma'_R}\cdots\phi_{\sigma'_1}$, where $\sum'$ means that all the fields share the same value of the site index and $\{\sigma_i, \sigma'_i\} \equiv \sigma_1\cdots\sigma_R, \sigma'_1\cdots\sigma'_R$. After doing a power expansion of $W[\phi^*, \phi]$ to quartic order, we obtain

that

$$S[\phi_\sigma^*,\phi_\sigma] = \int_0^\beta d\tau \sum_{\mathbf{r},\mathbf{r}'} \phi_\sigma^*(\mathbf{r}) T^{-1}_{\sigma\sigma'}(\mathbf{r}-\mathbf{r}')\phi_{\sigma'}(\mathbf{r}') - W[\phi_\sigma^*,\phi_\sigma]$$
$$= \int_0^\beta d\tau \sum_{\mathbf{r},\mathbf{r}'} \phi_\sigma^*(\mathbf{r}) T^{-1}_{\sigma\sigma'}(\mathbf{r}-\mathbf{r}')\phi_{\sigma'}(\mathbf{r}')$$
$$+ \int d\tau_1 d\tau_2 \sum_{\mathbf{r}} G_{\sigma\sigma}(\mathbf{r},\tau_1-\tau_2)\phi_\sigma^*(\mathbf{r},\tau_1)\phi_\sigma(\mathbf{r},\tau_2)$$
$$- \frac{1}{2!}\int \prod_{\alpha=1}^{4} d\tau_\alpha \sum_{\mathbf{r}} \chi_{\sigma\sigma'}(\mathbf{r},\tau_1,\tau_2,\tau_3,\tau_4)$$
$$\times \phi_\sigma^*(\tau_1)\phi_\sigma(\tau_2)\phi_{\sigma'}^*(\tau_3)\phi_{\sigma'}(\tau_4) + O(\phi^6), \tag{4}$$

where G is the local Green's function and χ is the two-particle vertex in the local limit, i.e., $t = 0$ (see details in Appendix B). However, starting from the above action, it is inconvenient to calculate physical quantities, such as the excitation spectrum or the momentum distribution. These difficulties can be circumvented through performing another Hubbard-Stratonovich transition to decouple the hopping term [27]. It is shown that the auxiliary field of this transformation has the same correlation functions as the original boson field (see details in Appendix C). Therefore, we can use the same notation for both fields. The partition function can thus be expressed as

$$Z = Z_0 \int D[\psi_\sigma^*,\psi_\sigma,\phi_\sigma^*,\phi_\sigma] \exp\left\{\int_0^\beta d\tau \sum_{\mathbf{r},\mathbf{r}'} \psi_\sigma^* T_{\sigma\sigma'}\psi_{\sigma'} - \left[\sum_{\sigma,\mathbf{r}}\int_0^\beta d\tau \psi_\sigma^*(\mathbf{r})\phi_\sigma(\mathbf{r}) + \text{c.c.}\right] + W[\phi_\sigma^*,\phi_\sigma]\right\}. \tag{5}$$

Integrating out the ϕ_σ field in Eq. (5), the effective action can be obtained,

$$S[\psi_\sigma^*,\psi_\sigma] = \int_0^\beta d\tau \sum_{\mathbf{r},\mathbf{r}'} \psi_\sigma^*(\mathbf{r},\tau)[-T_{\sigma\sigma'}(\mathbf{r}-\mathbf{r}')]\psi_{\sigma'}(\mathbf{r}',\tau)$$
$$+ \int_0^\beta d\tau_1 d\tau_2 \sum_{\mathbf{r}} \psi_\sigma^*(\mathbf{r},\tau_1)\big[-G^{-1}_{\sigma\sigma}(\tau_1-\tau_2)\big]$$
$$\times \psi_\sigma(\mathbf{r},\tau_2)$$
$$+ \frac{1}{2} g_{\sigma\sigma'} \int_0^\beta d\tau \sum_{\mathbf{r}} |\psi_\sigma(\mathbf{r},\tau)|^2 |\psi_{\sigma'}(\mathbf{r},\tau)|^2, \tag{6}$$

where $g_{\sigma\sigma'}$ captures the amplitude of the boson-boson interaction determined by the local two-particle vertex in its static limit (see details in Appendix B).

IV. PHASE DIAGRAM UNDER THE SADDLE-POINT APPROXIMATION

Starting from the above effective action, we first perform a saddle-point approximation to determine the ground state of our proposed system. The saddle-point action derived from Eq. (6) can be expressed as

$$S_{\text{saddle}} = -\bar{G}^{-1}_{ee}|\bar{\psi}_e|^2 - \bar{G}^{-1}_{oo}|\bar{\psi}_o|^2 - 4t\bar{\psi}_o^*\bar{\psi}_e - 4t\bar{\psi}_e^*\bar{\psi}_o - \frac{1}{4}\frac{\bar{\chi}_{ee}}{\bar{G}^4_{ee}}|\bar{\psi}_e|^4 - \frac{1}{4}\frac{\bar{\chi}_{oo}}{\bar{G}^4_{oo}}|\bar{\psi}_o|^4, \tag{7}$$

where $\bar{G}_{\sigma\sigma}$ and $\bar{\chi}_{\sigma\sigma}$ are the static limit of the single-particle Green's function and the two-particle vertex, respectively (see details in Appendix B). The saddle-point value $\bar{\psi}_\sigma$ can be obtained from minimizing S_{saddle}, and we obtain

$$n_{s,e} = \frac{\bar{G}^{-1}_{ee} + 4tc^{-1}}{g_{ee}} \quad \text{if } \bar{G}^{-1}_{ee} + 4tc^{-1} > 0,$$
$$n_{s,e} = 0 \quad \text{otherwise}, \tag{8}$$

$$n_{s,o} = \frac{\bar{G}^{-1}_{oo} + 4tc}{g_{oo}} \quad \text{if } \bar{G}^{-1}_{oo} + 4tc > 0,$$
$$n_{s,o} = 0 \quad \text{otherwise}, \tag{9}$$

where $n_{s,\sigma} = |\bar{\psi}_\sigma|^2$ is the superfluid density of the pseudospin σ component under the saddle-point approximation, and $c = |\bar{\psi}_e/\bar{\psi}_o|$. By utilizing an iterative algorithm to solve a complete set of self-consistent equations (2), (8), and (9), superfluid order parameters $\bar{\psi}_\sigma$ for even and odd lattice sites and the mean value of cavity field α can be determined. As defined in Eq. (2), α characterizes the average imbalance between even and odd lattice sites, which can be used as the order parameter describing the CDW order.

We display the phase diagram as a function of the lattice depth V_{2D} and detuning Δ_c in Fig. 1(a) to compare with the realistic experiments, such as the ETH experimental setup [22]. There are four different phases as shown in the phase diagram, which consists of a superfluid (SF) phase, a Mott insulator (MI) state, a charge-density-wave (CDW) state, and a supersolid (SS) phase. The difference among these four phases can be captured by order parameters defined above, for example, as shown in Fig. 1(b). A SF phase is characterized by finite and equal superfluid order parameters and vanishing even-odd imbalance indicated by $\alpha = 0$. It is quite different in the SS phase, where a finite even-odd imbalance and nonzero superfluid order parameters are observed. In both MI and CDW states, superfluid order parameters vanish. However, the presence of a finite even-odd imbalance $\alpha \neq 0$ distinguishes between MI and CDW states. The obtained phase diagram is consistent with other mean-field calculations [24,37]. However, the path integral approach constructed here can provide a systematic way beyond the mean-field approach for investigating the effect of high-order fluctuations. The unexpected results driven by the fluctuations will be unveiled below.

V. MANIPULATING GOLDSTONE MODES AT THE SS-CDW TRANSITION

Since typically fluctuations will play a dominant role in determining physical properties at the critical region, to explore the unexpected results arising from the fluctuations, we construct the critical theory describing the phase transition region as shown in Fig. 1(a). By performing both a spatial and a temporal gradient expansion of the action in Eq. (6), as well as the cumulant expansion in powers of ψ_σ [27,39,40],

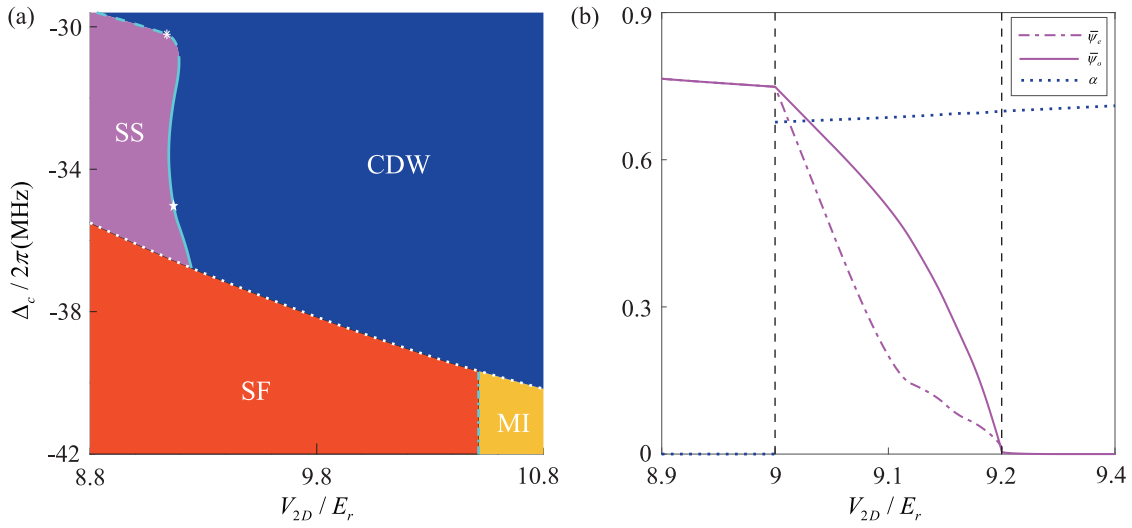

FIG. 1. (a) Zero-temperature phase diagram as a function of the lattice depth V_{2D} and Δ_c. The phase diagram shows four different phases, which are a superfluid (SF) phase, a Mott insulator (MI) state, a charge-density-wave (CDW) state, and a supersolid (SS) phase. The dashed and solid lines along the boundary between SS and CDW separate two distinct regions, where two different types of Goldstone modes (type I and type II) were found in its low-energy excitations, respectively. (b) Evolution of the different order parameters as a function of the lattice depth V_{2D} when $\Delta_c/2\pi = -36$ MHz. E_r is the recoil energy. Other parameters are chosen as $\mu = 0.42U$, $\kappa/\hbar = 2\pi \times 1.25$ MHz, and $N = 1 \times 10^4$. To compare with the realistic ^{87}Rb experiments, we choose the effective s-wave scattering length as $a_s = 120a_0$ (a_0 being the Bohr radius) and the lattice constant $2a = 785$ nm. Therefore, t/U can be estimated in the region of $t/U \in [0.074, 0.039]$ when varying V_{2D}/E_r from 8.8 to 10.8 as shown in (a).

the effective action can be rewritten as

$$\begin{aligned} S = \int_0^\beta d\tau \int d\mathbf{r}\{&[\psi_e^*(\mathbf{r},\tau) r_e \psi_e(\mathbf{r},\tau) + \psi_o^*(\mathbf{r},\tau) r_o \psi_o(\mathbf{r},\tau) \\ &- \psi_o^*(\mathbf{r},\tau) 4t \psi_e(\mathbf{r},\tau) - \psi_e^*(\mathbf{r},\tau) 4t \psi_o(\mathbf{r},\tau)] \\ &+ [K_{e1} \psi_e^*(\mathbf{r},\tau) \partial_\tau \psi_e(\mathbf{r},\tau) + K_{o1} \psi_o^*(\mathbf{r},\tau) \partial_\tau \psi_o(\mathbf{r},\tau)] \\ &+ [K_{e2} |\partial_\tau \psi_e(\mathbf{r},\tau)|^2 + K_{o2} |\partial_\tau \psi_o(\mathbf{r},\tau)|^2] \\ &+ [K_3 \nabla \psi_e^*(\mathbf{r},\tau) \nabla \psi_o(\mathbf{r},\tau) + K_3 \nabla \psi_o^*(\mathbf{r},\tau) \nabla \psi_e(\mathbf{r},\tau)] \\ &+ \frac{g_{ee}}{2} |\psi_e(\mathbf{r},\tau)|^4 + \frac{g_{oo}}{2} |\psi_o(\mathbf{r},\tau)|^4 + \frac{g_{eo}}{2} |\psi_e(\mathbf{r},\tau)|^2 \\ &\times |\psi_o(\mathbf{r},\tau)|^2 + \frac{g_{oe}}{2} |\psi_o(\mathbf{r},\tau)|^2 |\psi_e(\mathbf{r},\tau)|^2\}, \end{aligned} \tag{10}$$

where $r_e = -G_{ee}^{-1}(i\omega = 0)$, $r_o = -G_{oo}^{-1}(i\omega = 0)$, $K_{e1} = \frac{\partial G_{ee}^{-1}(i\omega)}{\partial(i\omega)}|_{i\omega=0}$, and $K_{o1} = \frac{\partial G_{oo}^{-1}(i\omega)}{\partial(i\omega)}|_{i\omega=0}$. $K_{e(o)2}$ and K_3 are the coefficients of the second-order temporal and spatial derivatives, respectively, which can be expressed in terms of the Green's function (see Appendix D for details).

Next, we introduce $\eta_\sigma(\mathbf{r},\tau) = \psi_\sigma(\mathbf{r},\tau) - \bar{\psi}_\sigma$ to describe the fluctuations. After expanding the action in Eq. (10) to the quadric order of fluctuation fields η_σ, we get

$$S = \frac{1}{2} \sum_{\mathbf{k},\omega} \tilde{\eta}^\dagger(\mathbf{k}, i\omega) M(\mathbf{k}, i\omega) \tilde{\eta}(\mathbf{k}, i\omega), \tag{11}$$

where $\tilde{\eta}^\dagger = [\eta_e^*(\mathbf{k}, i\omega), \eta_e(-\mathbf{k}, -i\omega), \eta_o^*(\mathbf{k}, i\omega), \eta_o(-\mathbf{k}, -i\omega)]$, and the matrix elements of M can be expressed as

$$\begin{aligned} M_{11} &= r_e - i\omega K_{e1} + K_{e2}\omega^2 + 2g_{ee}\bar{\psi}_e^2 + \frac{g_{eo}}{2}\bar{\psi}_o^2 + \frac{g_{oe}}{2}\bar{\psi}_o^2, \\ M_{22} &= r_e + i\omega K_{e1} + K_{e2}\omega^2 + 2g_{ee}\bar{\psi}_e^2 + \frac{g_{eo}}{2}\bar{\psi}_o^2 + \frac{g_{oe}}{2}\bar{\psi}_o^2, \\ M_{33} &= r_o - i\omega K_{o1} + K_{o2}\omega^2 + 2g_{oo}\bar{\psi}_o^2 + \frac{g_{eo}}{2}\bar{\psi}_e^2 + \frac{g_{oe}}{2}\bar{\psi}_e^2, \\ M_{44} &= r_o + i\omega K_{o1} + K_{o2}\omega^2 + 2g_{oo}\bar{\psi}_o^2 + \frac{g_{eo}}{2}\bar{\psi}_e^2 + \frac{g_{oe}}{2}\bar{\psi}_e^2, \\ M_{12} &= M_{21} = g_{ee}\bar{\psi}_e^2, \quad M_{34} = M_{43} = g_{oo}\bar{\psi}_o^2, \\ M_{13} &= M_{24} = M_{31} = M_{42} \\ &= -4t + K_3 k^2 + \frac{g_{eo}}{2}\bar{\psi}_e\bar{\psi}_o + \frac{g_{oe}}{2}\bar{\psi}_o\bar{\psi}_e, \\ M_{14} &= M_{23} = M_{32} = M_{41} = \frac{g_{eo}}{2}\bar{\psi}_e\bar{\psi}_o + \frac{g_{oe}}{2}\bar{\psi}_o\bar{\psi}_e. \end{aligned}$$

Therefore, the excitation spectrum at the critical region can be determined by solving the equation $\det[M(\mathbf{k}, i\omega)] = 0$. Eight excitation branches can thus be obtained, which form four positive-negative pairs due to the fact that Eq. (11) satisfies the time-reversal symmetry [41].

Here we focus on the transition from SS to CDW. In SS phase, there are two superfluid order parameters $\bar{\psi}_\sigma \equiv \sqrt{n_{s,\sigma}} e^{i\theta_\sigma}$ for even and odd lattice sites, where the amplitude and phase of the order parameter emerge as two independent degrees of freedom, instead of being conjugate to each other. The two phase fluctuation modes will be coupled to each other due to the presence of hopping between even and odd lattice sites and split into one (gapless) Goldstone mode associated with the overall phase $\theta_o + \theta_e$ plus a gapped mode linking to the relative phase $\theta_o - \theta_e$. By contrast, the amplitude fluctuations lead to the Higgs modes (two higher modes obtained from $\det[M(\mathbf{k}, i\omega)] = 0$).

At the transition from SS to CDW, we find the new feature of the gapless Goldstone mode. Previous studies show that the slight modulation of density imbalance induced by the superradiant cavity light has a negligible effect on the

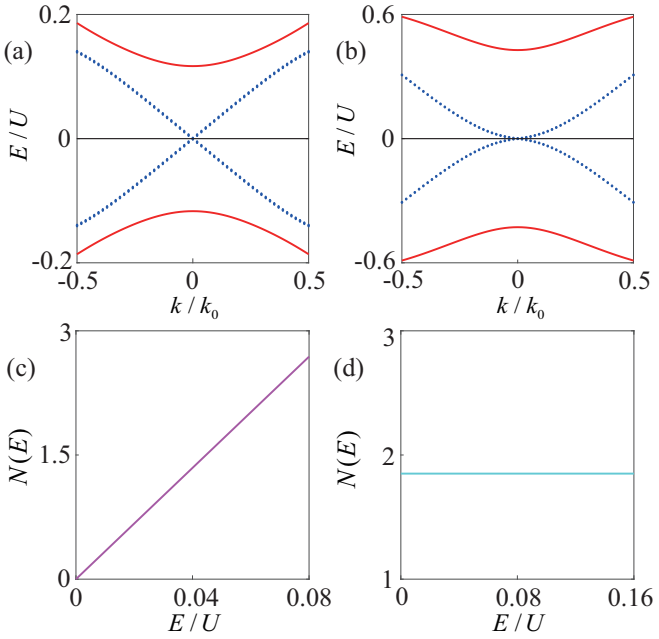

FIG. 2. Energy spectra for the two phase modes (a) when $V_{2D}/E_r = 9.1$, $\Delta_c/2\pi = -30.2$ MHz as indicated by "$*$" in Fig. 1(a), and (b) when $V_{2D}/E_r = 9.14$, $\Delta_c/2\pi = -35$ MHz as labeled by "$\star$" in Fig. 1(a). Other parameters are the same as in Fig. 1. (c) and (d) Density of states (DOS) defined in the main text for type I and type II Goldstone modes, corresponding to the cases in (a) and (b), respectively.

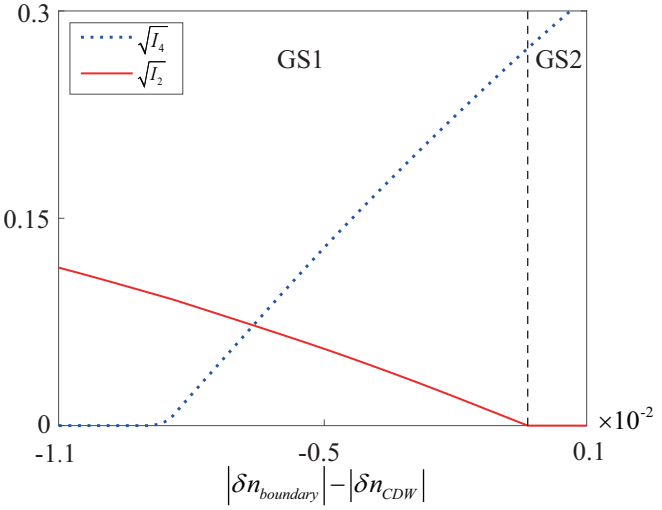

FIG. 3. The coefficients I_2 and I_4 in $E^+_{\text{Goldstone}}$ [Eq. (12)] as a function of density imbalance modulation when varying the system along the phase boundary between SS and CDW as shown in Fig. 1(a). The dashed line separates the regions with type I and type II Goldstone modes, respectively. $\delta n_{\text{boundary}}$ and δn_{CDW} describe the atom density imbalance between even and odd sites, when considering the system along the phase boundary and in CDW, respectively. Other parameters are chosen the same as in Fig. 1. For the parameter regime considered here, the average density of even and odd lattice sites in the CDW phase is 0 and 2, respectively, which corresponds to $|\delta n_{\text{CDW}}| = 2$ by definition.

low-energy excitations [24]. Here we first show that at the transition from SS to CDW, even such tiny modulation of density imbalance will result in a dramatic effect on the excitations. Distinct from several types of the mean-field approach [24,37], such as employing the Gutzwiller ansatz, the critical theory constructed in Eq. (10) can unveil the dominant role of fluctuations. It is found that tuning the system along the phase boundary between SS and CDW as shown in Fig. 1(a) can switch between two types of Goldstone modes in its low-energy excitation spectrum, i.e., type I and type II with odd and even power energy-momentum dispersion (as shown in Fig. 2), respectively.

To further understand the underlying physics, we analytically solve the equation $\det[M(\mathbf{k}, i\omega)] = 0$ and find that in the long wave limit, the low-energy excitation (lowest positive branch) can be approximately expressed as (see details in Appendix E)

$$E^+_{\text{Goldstone}} \simeq \sqrt{I_2}k + \sqrt{I_4}k^2. \tag{12}$$

Therefore, the switching from type I to type II Goldstone modes can be achieved by changing the coefficients I_2 and I_4. Around the transition from SS to CDW, the strong quantum fluctuations show a dramatic effect. They make even the slight modulation of density imbalance play a dominant role in determining I_2 and I_4. As shown in Fig. 3, it leads to two distinct regions: (I) $I_2 \neq 0$, and (II) $I_2 = 0$ and $I_4 \neq 0$, which correspond to type I and type II Goldstone modes, respectively. Such an unusual effect of the fluctuation will disappear when departing from the critical region. For instance, inside the SS-phase, the dispersion of the Goldstone mode will remain as a linear function. To distinguish these two different types of Goldstone modes, we calculate their corresponding density of states (DOS) as $N(E) = \frac{1}{N}\sum_{\mathbf{k}} \delta(E - E^+_{\text{Goldstone}})$, which is directly related to the Bragg spectroscopy signal [42]. As shown in Fig. 2, with linear dispersion (type I), we find $N(E) \propto E$ when $E \to 0$. It is distinct from the quadratic dispersion (type II), where $N(E)$ is a constant when $E \to 0$. As we propose above, type I and type II Goldstone modes can be distinguished from their distinct behavior of DOS in the low-energy limit, which is linked to the low-energy responses in the Bragg spectroscopy experiments (typically $\omega/2\pi \ll 10$ kHz [43]). To compare with the realistic ^{87}Rb experiments, we choose the effective s-wave scattering length as $a_s = 120a_0$, lattice constant $2a = 785$ nm, and other parameters to be the same as in Figs. 2(c) and 2(d). Therefore, the energy region as shown in Figs. 2(c) and 2(d) is below a few hundred Hz, which makes the low-energy signal in the Bragg spectroscopy [9] experimentally accessible.

VI. CONCLUSION

By performing two successive Hubbard-Stratonovich transformations, we have developed an effective field theory to study a bosonic lattice gas inside a cavity in the strongly interacting regime. Through taking into account the quantum fluctuations, we first find that the slight modulation of density imbalance, neglected in the previous studies, leads to dramatic changes in the behavior of low-energy excitations. The switching between type I and type II Goldstone modes

can be driven along the SS-CDW transition. Our findings would bridge the cavity light and strongly interacting quantum matters, and it may open up a new direction in this field.

ACKNOWLEDGMENTS

This work is supported by the National Key R&D Program of China (2021YFA1401700), NSFC (Grants No. 12074305, No. 12147137, No. 11774282, and No. 11950410491), the National Key Research and Development Program of China (2018YFA0307600), the Fundamental Research Funds for the Central Universities and Cyrus Tang Foundation Young Scholar Program (H.W., S.L., M.A., and B.L.) and by the AFOSR Grant No. FA9550-16-1-0006, the MURI-ARO Grant No. W911NF17-1-0323 through UC Santa Barbara, and the Shanghai Municipal Science and Technology Major Project through the Shanghai Research Center for Quantum Sciences (Grant No. 2019SHZDZX01) (W.V.L.). We also thank the HPC platform of Xi'An Jiaotong University, where our numerical calculations were performed.

APPENDIX A: HOPPING TERM

The hopping term in Eq. (1) can be written as

$$\begin{aligned} H_{\text{hop}} &= \sum_{\mathbf{r},\mathbf{r}'} - T_{\sigma\sigma'}(\mathbf{r}-\mathbf{r}')\psi^\dagger_\sigma(\mathbf{r})\psi_{\sigma'}(\mathbf{r}') \\ &= -\sum_{\mathbf{r}}\Psi^\dagger(\mathbf{r})T_0\Psi(\mathbf{r}) - \sum_{\mathbf{r}}\Psi^\dagger(\mathbf{r})T_{1x}\Psi(\mathbf{r}+\mathbf{e}_x) \\ &\quad -\sum_{\mathbf{r}}\Psi^\dagger(\mathbf{r})T'_{1x}\Psi(\mathbf{r}-\mathbf{e}_x) - \sum_{\mathbf{r}}\Psi^\dagger(\mathbf{r})T_{1z}\Psi(\mathbf{r}+\mathbf{e}_z) \\ &\quad -\sum_{\mathbf{r}}\Psi^\dagger(\mathbf{r})T'_{1z}\Psi(\mathbf{r}-\mathbf{e}_z) - \sum_{\mathbf{r}}\Psi^\dagger(\mathbf{r})T_2\Psi(\mathbf{r}+\mathbf{e}_x-\mathbf{e}_z) \\ &\quad -\sum_{\mathbf{r}}\Psi^\dagger(\mathbf{r})T'_2\Psi(\mathbf{r}-\mathbf{e}_x+\mathbf{e}_z), \end{aligned} \tag{A1}$$

where $\Psi(\mathbf{r}) = [\psi_e(\mathbf{r}) \quad \psi_o(\mathbf{r})]^T$, and $\sigma = e, o$ stands for even and odd sites, respectively. $T_{\sigma\sigma'}$ is the hopping matrix, and $\mathbf{r}, \mathbf{r}'$ label the location of the unit cell as shown in Fig. 4. The hopping matrices can be expressed as

$$\begin{aligned} T_0 &= \begin{pmatrix} 0 & t \\ t & 0 \end{pmatrix}, \\ T_{1x} = T'_{1z} = T_2 &= \begin{pmatrix} 0 & t \\ 0 & 0 \end{pmatrix}, \\ T'_{1x} = T_{1z} = T'_2 &= \begin{pmatrix} 0 & 0 \\ t & 0 \end{pmatrix}. \end{aligned} \tag{A2}$$

In the momentum space, the hopping term H_{hop} can be written as

$$H_{\text{hop}}(\mathbf{k}) = \sum_{\mathbf{k}}[\psi^\dagger_e(\mathbf{k}), \psi^\dagger_o(\mathbf{k})]\begin{bmatrix} 0 & \epsilon_{eo}(\mathbf{k}) \\ \epsilon_{oe}(\mathbf{k}) & 0 \end{bmatrix}\begin{bmatrix} \psi_e(\mathbf{k}) \\ \psi_o(\mathbf{k}) \end{bmatrix}, \tag{A3}$$

where a is the lattice constant, and the band dispersion $\epsilon_{eo}(\mathbf{k}) = -t\{1 + e^{ik_x\sqrt{2}a} + e^{-ik_z\sqrt{2}a} + e^{ik_x\sqrt{2}a-ik_z\sqrt{2}a}\}$, $\epsilon_{oe}(\mathbf{k}) = -t\{1 + e^{-ik_x\sqrt{2}a} + e^{ik_z\sqrt{2}a} + e^{-ik_x\sqrt{2}a+ik_z\sqrt{2}a}\}$.

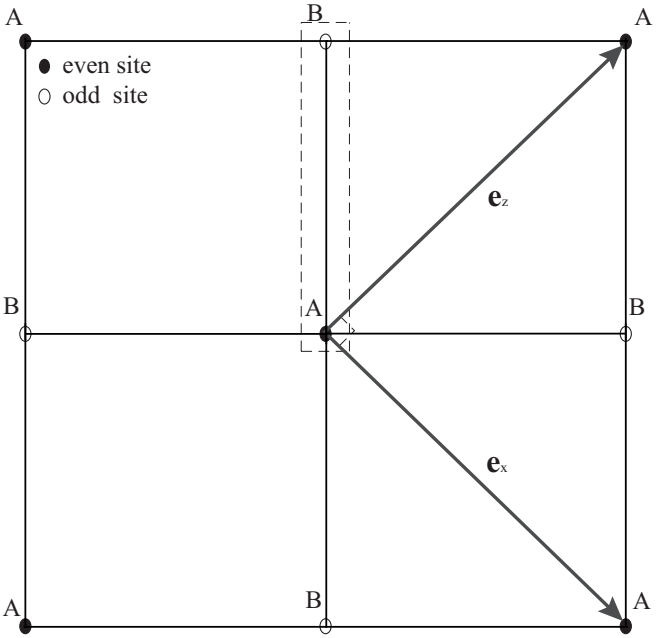

FIG. 4. Schematic picture of a two-dimensional checkerboard lattice. Here A and B stand for two different sites in one unit cell (even and odd sites), and $\mathbf{e_x}$ and $\mathbf{e_z}$ are the primitive unit vectors.

APPENDIX B: LOCAL SINGLE-PARTICLE AND TWO-PARTICLE GREEN'S FUNCTION

In the absence of hopping, i.e., $t = 0$, the local Hamiltonian can be defined from Eq. (1) as $H_0 = \frac{U}{2}\sum_{\mathbf{r},\sigma} n_\sigma(\mathbf{r})[n_\sigma(\mathbf{r}) - 1] - \sum_{\mathbf{r},\sigma}\mu_\sigma n_\sigma(\mathbf{r}) - \delta_c|\alpha|^2$ with the energy detuning δ_c. Then, the local single-particle Green's function can be calculated in the operator representation via the occupation number basis, for instance,

$$G_{ee}(\tau) = -\left\langle T_\tau \hat{\psi}_e(\tau)\psi^\dagger_e(0)\right\rangle = -\frac{1}{Z_0}\text{Tr}[e^{-(\beta-\tau)H_0}\hat{\psi}_e e^{-\tau H_0}\psi^\dagger_e], \tag{B1}$$

where $Z_0 = \text{Tr}\, e^{-\beta H_0}$ and $|n_e n_o\rangle = \frac{(\hat{\psi}^\dagger_e)^{n_e}(\hat{\psi}^\dagger_o)^{n_o}}{\sqrt{n_e! n_o!}}|0\rangle$ is the eigenbasis of the local Hamiltonian H_0 with eigenvalue $\varepsilon_{n_e,n_o} = \frac{U}{2}n_o(n_o-1) + \frac{U}{2}n_e(n_e-1) - \mu_o n_o - \mu_e n_e - \delta_c|\alpha|^2$. After implementing the Fourier transform, the above correlator can be expressed as

$$\begin{aligned} G_{ee}(i\omega) &= \int_0^\beta d\tau\, e^{i\omega\tau}G_{ee}(\tau) \\ &= -\frac{1}{Z_0}\sum_{n_e,n_o}(n_e+1)\frac{e^{-\beta\varepsilon_{n_e+1,n_o}} - e^{-\beta\varepsilon_{n_e,n_o}}}{i\omega + \varepsilon_{n_e,n_o} - \varepsilon_{n_e+1,n_o}}. \end{aligned} \tag{B2}$$

In the low -temperature limit $T \to 0(\beta U \gg 1)$, the exponential term in Eq. (B2) selects out the ground state of the local Hamiltonian, and contributions of other states are suppressed. Therefore, G_{ee} can be calculated as

$$G_{ee}(i\omega) = \frac{\bar{n}_e + 1}{i\omega + \varepsilon_{\bar{n}_e,0} - \varepsilon_{\bar{n}_e+1,0}} - \frac{\bar{n}_e}{i\omega + \varepsilon_{\bar{n}_e-1,0} - \varepsilon_{\bar{n}_e,0}}, \tag{B3}$$

where $\bar{n}_e$ and $\bar{n}_o$ can be determined through minimizing the ground-state energy $\varepsilon_{\bar{n}_e,\bar{n}_o} = \min_{n_e,n_o}\varepsilon_{n_e,n_o}$. In the same way, we can also obtain the local Green's function G_{oo} as

$$G_{oo}(i\omega) = \frac{\bar{n}_o + 1}{i\omega + \varepsilon_{0,\bar{n}_o} - \varepsilon_{0,\bar{n}_o+1}} - \frac{\bar{n}_o}{i\omega + \varepsilon_{0,\bar{n}_o-1} - \varepsilon_{0,\bar{n}_o}}. \tag{B4}$$

The two-particle Green's function can be calculated in a similar way as

$$\chi_{\sigma\sigma'}(\tau_1, \tau_2, \tau_3, 0) = \left\langle T_\tau \psi_\sigma(\tau_1)\psi^\dagger_\sigma(\tau_2)\psi_{\sigma'}(\tau_3)\psi^\dagger_{\sigma'}(0)\right\rangle, \tag{B5}$$

where $\sigma = e, o$. To calculate the parameter $g_{\sigma\sigma'}$ in the static limit, we only consider the time average of the connected part of $\chi_{\sigma\sigma'}$. Then, the diagonal part can be calculated as

$$\begin{aligned}
\bar{\chi}_{ee} &= \int_0^\beta d\tau_1 d\tau_2 d\tau_3 \left\langle T_\tau \psi_e(\tau_1)\psi^\dagger_e(\tau_2)\psi_e(\tau_3)\psi^\dagger_e(0)\right\rangle^c \\
&= \int_0^\beta d\tau_1 d\tau_2 d\tau_3 \chi_{ee}(\tau_1, \tau_2, \tau_3, 0) - 2\beta[G_{ee}(i\omega = 0)]^2 \\
&= \frac{-4(\bar{n}_e + 1)(\bar{n}_e + 2)}{\left(\varepsilon_{\bar{n}_e,0} - \varepsilon_{\bar{n}_e+1,0}\right)^2\left(\varepsilon_{\bar{n}_e,0} - \varepsilon_{\bar{n}_e+2,0}\right)} + \frac{-4\bar{n}_e(\bar{n}_e - 1)}{\left(\varepsilon_{\bar{n}_e,0} - \varepsilon_{\bar{n}_e-1,0}\right)^2\left(\varepsilon_{\bar{n}_e,0} - \varepsilon_{\bar{n}_e-2,0}\right)} + \frac{-4\bar{n}_e(\bar{n}_e + 1)}{\left(\varepsilon_{\bar{n}_e-1,0} - \varepsilon_{\bar{n}_e,0}\right)^2\left(\varepsilon_{\bar{n}_e+1,0} - \varepsilon_{\bar{n}_e,0}\right)} \\
&\quad + \frac{4\bar{n}_e(\bar{n}_e + 1)}{\left(\varepsilon_{\bar{n}_e,0} - \varepsilon_{\bar{n}_e+1,0}\right)^2\left(\varepsilon_{\bar{n}_e,0} - \varepsilon_{\bar{n}_e-1,0}\right)} + \frac{4(\bar{n}_e + 1)^2}{\left(\varepsilon_{\bar{n}_e,0} - \varepsilon_{\bar{n}_e+1,0}\right)^3} + \frac{-4\bar{n}_e^2}{\left(\varepsilon_{\bar{n}_e-1,0} - \varepsilon_{\bar{n}_e,0}\right)^3},
\end{aligned} \tag{B6}$$

with the upper index "c" labeling the connected part of the two-particle Green's function, and

$$\begin{aligned}
\chi_{ee}(\tau_1, \tau_2, \tau_3, 0) = \frac{1}{Z_0}\sum_{n_e=0}^{\infty} e^{-\beta\varepsilon_{n_e,0}} \{ &\theta(\tau_1 - \tau_2)\theta(\tau_2 - \tau_3) e^{\tau_1(\varepsilon_{n_e,0} - \varepsilon_{n_e+1,0}) + \tau_2(\varepsilon_{n_e+1,0} - \varepsilon_{n_e,0}) + \tau_3(\varepsilon_{n_e,0} - \varepsilon_{n_e+1,0})}(n_e + 1)^2 \\
&+ \theta(\tau_1 - \tau_3)\theta(\tau_3 - \tau_2) e^{\tau_1(\varepsilon_{n_e,0} - \varepsilon_{n_e+1,0}) + \tau_2(\varepsilon_{n_e+2,0} - \varepsilon_{n_e+1,0}) + \tau_3(\varepsilon_{n_e+1,0} - \varepsilon_{n_e+2,0})}(n_e + 1)(n_e + 2) \\
&+ \theta(\tau_3 - \tau_1)\theta(\tau_1 - \tau_2) e^{\tau_1(\varepsilon_{n_e+1,0} - \varepsilon_{n_e+2,0}) + \tau_2(\varepsilon_{n_e+2,0} - \varepsilon_{n_e+1,0}) + \tau_3(\varepsilon_{n_e,0} - \varepsilon_{n_e+1,0})}(n_e + 1)(n_e + 2) \\
&+ \theta(\tau_2 - \tau_1)\theta(\tau_1 - \tau_3) e^{\tau_1(\varepsilon_{n_e-1,0} - \varepsilon_{n_e,0}) + \tau_2(\varepsilon_{n_e,0} - \varepsilon_{n_e-1,0}) + \tau_3(\varepsilon_{n_e,0} - \varepsilon_{n_e+1,0})}(n_e + 1)n_e \\
&+ \theta(\tau_2 - \tau_3)\theta(\tau_3 - \tau_1) e^{\tau_1(\varepsilon_{n_e,0} - \varepsilon_{n_e+1,0}) + \tau_2(\varepsilon_{n_e,0} - \varepsilon_{n_e-1,0}) + \tau_3(\varepsilon_{n_e-1,0} - \varepsilon_{n_e,0})}(n_e + 1)n_e \\
&+ \theta(\tau_3 - \tau_2)\theta(\tau_2 - \tau_1) e^{\tau_1(\varepsilon_{n_e,0} - \varepsilon_{n_e+1,0}) + \tau_2(\varepsilon_{n_e+1,0} - \varepsilon_{n_e,0}) + \tau_3(\varepsilon_{n_e,0} - \varepsilon_{n_e+1,0})}(n_e + 1)^2 \}.
\end{aligned}$$

Similarly, the other diagonal part can also be calculated as follows:

$$\begin{aligned}
\bar{\chi}_{oo} &= \int_0^\beta d\tau_1 d\tau_2 d\tau_3 \chi_{oo}(\tau_1, \tau_2, \tau_3, 0) - 2\beta[G_{oo}(i\omega = 0)]^2 \\
&= \frac{-4(\bar{n}_o + 1)(\bar{n}_o + 2)}{\left(\varepsilon_{0,\bar{n}_o} - \varepsilon_{0,\bar{n}_o+1}\right)^2\left(\varepsilon_{0,\bar{n}_o} - \varepsilon_{0,\bar{n}_o+2}\right)} + \frac{-4\bar{n}_o(\bar{n}_o - 1)}{\left(\varepsilon_{0,\bar{n}_o} - \varepsilon_{0,\bar{n}_o-1}\right)^2\left(\varepsilon_{0,\bar{n}_o} - \varepsilon_{0,\bar{n}_o-2}\right)} \\
&\quad + \frac{-4\bar{n}_o(\bar{n}_o + 1)}{\left(\varepsilon_{0,\bar{n}_o-1} - \varepsilon_{0,\bar{n}_o}\right)^2\left(\varepsilon_{0,\bar{n}_o+1} - \varepsilon_{0,\bar{n}_o}\right)} + \frac{4\bar{n}_o(\bar{n}_o + 1)}{\left(\varepsilon_{0,\bar{n}_o} - \varepsilon_{0,\bar{n}_o+1}\right)^2\left(\varepsilon_{0,\bar{n}_o} - \varepsilon_{0,\bar{n}_o-1}\right)} \\
&\quad + \frac{4(\bar{n}_o + 1)^2}{\left(\varepsilon_{0,\bar{n}_o} - \varepsilon_{0,\bar{n}_o+1}\right)^3} + \frac{-4\bar{n}_o^2}{\left(\varepsilon_{0,\bar{n}_o-1} - \varepsilon_{0,\bar{n}_o}\right)^3}.
\end{aligned} \tag{B7}$$

In a similar way, we can obtain the off-diagonal part in the static limit as

$$\bar{\chi}_{eo} = \bar{n}_e f_1 + (\bar{n}_e + 1)f_2 + \bar{n}_e f_3 + (\bar{n}_e + 1)f_4, \tag{B8}$$

with

$$\begin{aligned}
f_1 = \Bigg\{ &\frac{-\bar{n}_o}{\left(\varepsilon_{\bar{n}_e,\bar{n}_o} - \varepsilon_{\bar{n}_e,\bar{n}_o-1}\right)^2\left(\varepsilon_{\bar{n}_e,\bar{n}_o} - \varepsilon_{\bar{n}_e-1,\bar{n}_o-1}\right)} + \frac{-\bar{n}_o}{\left(\varepsilon_{\bar{n}_e,\bar{n}_o} - \varepsilon_{\bar{n}_e-1,\bar{n}_o}\right)^2\left(\varepsilon_{\bar{n}_e,\bar{n}_o} - \varepsilon_{\bar{n}_e-1,\bar{n}_o-1}\right)} \\
&+ \frac{\bar{n}_o}{\left(\varepsilon_{\bar{n}_e,\bar{n}_o} - \varepsilon_{\bar{n}_e,\bar{n}_o-1}\right)^2\left(\varepsilon_{\bar{n}_e,\bar{n}_o} - \varepsilon_{\bar{n}_e-1,\bar{n}_o}\right)} + \frac{\bar{n}_o}{\left(\varepsilon_{\bar{n}_e,\bar{n}_o} - \varepsilon_{\bar{n}_e-1,\bar{n}_o}\right)^2\left(\varepsilon_{\bar{n}_e,\bar{n}_o} - \varepsilon_{\bar{n}_e,\bar{n}_o-1}\right)} \\
&+ \frac{-2\bar{n}_o}{\left(\varepsilon_{\bar{n}_e,\bar{n}_o} - \varepsilon_{\bar{n}_e-1,\bar{n}_o}\right)\left(\varepsilon_{\bar{n}_e,\bar{n}_o} - \varepsilon_{\bar{n}_e,\bar{n}_o-1}\right)\left(\varepsilon_{\bar{n}_e,\bar{n}_o} - \varepsilon_{\bar{n}_e-1,\bar{n}_o-1}\right)} \Bigg\},
\end{aligned}$$

$$f_2 = \left\{ \frac{-\bar{n}_o}{\left(\varepsilon_{\bar{n}_e,\bar{n}_o} - \varepsilon_{\bar{n}_e,\bar{n}_o-1}\right)^2\left(\varepsilon_{\bar{n}_e,\bar{n}_o} - \varepsilon_{\bar{n}_e+1,\bar{n}_o-1}\right)} + \frac{-\bar{n}_o}{\left(\varepsilon_{\bar{n}_e,\bar{n}_o} - \varepsilon_{\bar{n}_e+1,\bar{n}_o}\right)^2\left(\varepsilon_{\bar{n}_e,\bar{n}_o} - \varepsilon_{\bar{n}_e+1,\bar{n}_o-1}\right)} \right.$$

$$+\frac{\bar{n}_o}{\left(\varepsilon_{\bar{n}_e,\bar{n}_o-1}-\varepsilon_{\bar{n}_e,\bar{n}_o}\right)^2\left(\varepsilon_{\bar{n}_e,\bar{n}_o}-\varepsilon_{\bar{n}_e+1,\bar{n}_o}\right)}+\frac{\bar{n}_o}{\left(\varepsilon_{\bar{n}_e,\bar{n}_o}-\varepsilon_{\bar{n}_e+1,\bar{n}_o}\right)^2\left(\varepsilon_{\bar{n}_e,\bar{n}_o}-\varepsilon_{\bar{n}_e,\bar{n}_o-1}\right)}$$
$$+\frac{-2\bar{n}_o}{\left(\varepsilon_{\bar{n}_e,\bar{n}_o}-\varepsilon_{\bar{n}_e+1,\bar{n}_o}\right)\left(\varepsilon_{\bar{n}_e,\bar{n}_o}-\varepsilon_{\bar{n}_e+1,\bar{n}_o-1}\right)\left(\varepsilon_{\bar{n}_e,\bar{n}_o}-\varepsilon_{\bar{n}_e,\bar{n}_o-1}\right)}\Bigg\},$$

$$f_3=\Bigg\{\frac{-(\bar{n}_o+1)}{\left(\varepsilon_{\bar{n}_e,\bar{n}_o}-\varepsilon_{\bar{n}_e-1,\bar{n}_o}\right)^2\left(\varepsilon_{\bar{n}_e,\bar{n}_o}-\varepsilon_{\bar{n}_e-1,\bar{n}_o+1}\right)}+\frac{(\bar{n}_o+1)}{\left(\varepsilon_{\bar{n}_e,\bar{n}_o}-\varepsilon_{\bar{n}_e-1,\bar{n}_o}\right)^2\left(\varepsilon_{\bar{n}_e,\bar{n}_o}-\varepsilon_{\bar{n}_e,\bar{n}_o+1}\right)}$$
$$+\frac{(\bar{n}_o+1)}{\left(\varepsilon_{\bar{n}_e,\bar{n}_o}-\varepsilon_{\bar{n}_e,\bar{n}_o+1}\right)^2\left(\varepsilon_{\bar{n}_e,\bar{n}_o}-\varepsilon_{\bar{n}_e-1,\bar{n}_o}\right)}+\frac{-(\bar{n}_o+1)}{\left(\varepsilon_{\bar{n}_e,\bar{n}_o}-\varepsilon_{\bar{n}_e,\bar{n}_o+1}\right)^2\left(\varepsilon_{\bar{n}_e,\bar{n}_o}-\varepsilon_{\bar{n}_e-1,\bar{n}_o+1}\right)}$$
$$+\frac{-2(\bar{n}_o+1)}{\left(\varepsilon_{\bar{n}_e,\bar{n}_o}-\varepsilon_{\bar{n}_e-1,\bar{n}_o}\right)\left(\varepsilon_{\bar{n}_e,\bar{n}_o}-\varepsilon_{\bar{n}_e,\bar{n}_o+1}\right)\left(\varepsilon_{\bar{n}_e,\bar{n}_o}-\varepsilon_{\bar{n}_e-1,\bar{n}_o+1}\right)}\Bigg\},$$

$$f_4=\Bigg\{\frac{(\bar{n}_o+1)}{\left(\varepsilon_{\bar{n}_e,\bar{n}_o}-\varepsilon_{\bar{n}_e,\bar{n}_o+1}\right)^2\left(\varepsilon_{\bar{n}_e,\bar{n}_o}-\varepsilon_{\bar{n}_e+1,\bar{n}_o}\right)}+\frac{(\bar{n}_o+1)}{\left(\varepsilon_{\bar{n}_e,\bar{n}_o}-\varepsilon_{\bar{n}_e+1,\bar{n}_o}\right)^2\left(\varepsilon_{\bar{n}_e,\bar{n}_o}-\varepsilon_{\bar{n}_e,\bar{n}_o+1}\right)}$$
$$+\frac{-(\bar{n}_o+1)}{\left(\varepsilon_{\bar{n}_e,\bar{n}_o}-\varepsilon_{\bar{n}_e,\bar{n}_o+1}\right)^2\left(\varepsilon_{\bar{n}_e,\bar{n}_o}-\varepsilon_{\bar{n}_e+1,\bar{n}_o+1}\right)}+\frac{-(\bar{n}_o+1)}{\left(\varepsilon_{\bar{n}_e,\bar{n}_o}-\varepsilon_{\bar{n}_e+1,\bar{n}_o}\right)^2\left(\varepsilon_{\bar{n}_e,\bar{n}_o}-\varepsilon_{\bar{n}_e+1,\bar{n}_o+1}\right)}$$
$$+\frac{-2(\bar{n}_o+1)}{\left(\varepsilon_{\bar{n}_e,\bar{n}_o}-\varepsilon_{\bar{n}_e+1,\bar{n}_o}\right)\left(\varepsilon_{\bar{n}_e,\bar{n}_o}-\varepsilon_{\bar{n}_e+1,\bar{n}_o+1}\right)\left(\varepsilon_{\bar{n}_e,\bar{n}_o}-\varepsilon_{\bar{n}_e,\bar{n}_o+1}\right)}\Bigg\}.$$

Up to this point, we have obtained the two-point and four-point correlators from the local Hamiltonian. Then, $g_{\sigma\sigma'}$ in Eq. (6) of the main text can be determined by the two-particle vertex in the static limit, which can be written as

$$g_{\sigma\sigma'}=\frac{-\bar{\chi}_{\sigma\sigma'}}{(\bar{G}_{\sigma\sigma}\bar{G}_{\sigma'\sigma'})^2+(\bar{G}_{\sigma\sigma})^4\delta_{\sigma\sigma'}}, \tag{B9}$$

where $\bar{G}_{\sigma\sigma}=G_{\sigma\sigma}(i\omega=0)$.

APPENDIX C: DOUBLE HUBBARD-STRATONOVICH TRANSFORMATION

The connected correlators of the original boson fields ψ_σ can be obtained from the generating function

$$Z[J^*,J]=\int D[\psi^*,\psi]\exp\{\psi^*_\sigma T_{\sigma\sigma'}\psi_{\sigma'}-S_0[\psi^*_\sigma,\psi_\sigma]+[(J|\psi)+\text{c.c.}]\}, \tag{C1}$$

where J, J^* are external sources and $(J|\psi)=\sum_{\sigma,\text{r}}\int_0^\beta d\tau J^*_\sigma(\mathbf{r})\psi_\sigma(\mathbf{r})$. Introducing the first Hubbard-Stratonovich transformation with auxiliary field ϕ,

$$Z[J^*,J]=\int D[\psi^*,\psi;\phi^*,\phi]\exp\left\{-\phi^*_\sigma T^{-1}_{\sigma\sigma'}\phi_{\sigma'}-S_0[\psi^*_\sigma,\psi_\sigma]+[(\phi|\psi)+\text{c.c.}]+[(J|\psi)+\text{c.c.}]\right\}. \tag{C2}$$

After a shift $\phi_\sigma\longrightarrow\phi_\sigma-J_\sigma$, $\phi^*_\sigma\longrightarrow\phi^*_\sigma-J^*_\sigma$, we obtain

$$Z[J^*,J]=\int D[\psi^*,\psi;\phi^*,\phi]\exp\left\{-(\phi^*_\sigma-J^*_\sigma)T^{-1}_{\sigma\sigma'}(\phi_{\sigma'}-J_{\sigma'})-S_0[\psi^*_\sigma,\psi_\sigma]+[(\phi|\psi)+\text{c.c.}]\right\}. \tag{C3}$$

Integrating ψ_σ fields, we then obtain

$$Z[J^*,J]=Z_0\int D[\phi^*,\phi]\exp\left\{-(\phi^*_\sigma-J^*_\sigma)T^{-1}_{\sigma\sigma'}(\phi_{\sigma'}-J_{\sigma'})+W[\phi^*_\sigma,\phi_\sigma]\right\}. \tag{C4}$$

Next, applying the second Hubbard-Stratonovich transformation with auxiliary field ψ', we obtain

$$\begin{aligned}Z[J^*,J]&=Z_0\int D[\phi^*,\phi;\psi'^*,\psi']\exp\{\psi'^*_\sigma T_{\sigma\sigma'}\psi'_\sigma-[(\psi'|\phi-J)+\text{c.c.}]+W[\phi^*_\sigma,\phi_\sigma]\}\\&=Z_0\int D[\phi^*,\phi;\psi'^*,\psi']\exp\{\psi'^*_\sigma T_{\sigma\sigma'}\psi'_\sigma-[(\psi'|\phi)+\text{c.c.}]+[(\psi'|J)+\text{c.c.}]+W[\phi^*_\sigma,\phi_\sigma]\}.\end{aligned} \tag{C5}$$

After integrating ϕ_σ fields, we get

$$Z[J^*,J]=Z_0\int D[\psi'^*,\psi']\exp\{\psi'^*_\sigma T_{\sigma\sigma'}\psi'_\sigma+\tilde{W}[\psi'^*_\sigma,\psi'_\sigma]+[(\psi'|J)+\text{c.c.}]\}. \tag{C6}$$

From the above equation, we prove that $Z[J^*, J]$ is also the generating function of the ψ'_σ field, which is equal to the generating function of the original ψ field. This proves that the connected correlators of ψ'_σ are the same as that of ψ_σ. Therefore, ψ'_σ is identified with the original boson field ψ_σ. We can thus use the same notation for both fields.

APPENDIX D: COEFFICIENTS OF THE EFFECTIVE ACTION AT THE CRITICAL REGION

To obtain the effective action at the critical region, we first rewrite the action Eq. (6) in the main text in momentum space as

$$\begin{aligned} S_k = &\sum_{\mathbf{k},\omega} \psi_e^*(\mathbf{k},i\omega)\big[-G_{ee}^{-1}(i\omega)\big]\psi_e(\mathbf{k},i\omega) + \psi_o^*(\mathbf{k},i\omega)\big[-G_{oo}^{-1}(i\omega)\big]\psi_o(\mathbf{k},i\omega) \\ &+ \psi_e^*(\mathbf{k},i\omega)\epsilon_{eo}(\mathbf{k})\psi_o(\mathbf{k},i\omega) + \psi_o^*(\mathbf{k},i\omega)\epsilon_{oe}(\mathbf{k})\psi_e(\mathbf{k},i\omega) + \frac{1}{2}g_{ee}|\psi_e(\mathbf{k},i\omega)|^4 \\ &+ \frac{1}{2}g_{oo}|\psi_o(\mathbf{k},i\omega)|^4 + \frac{1}{2}g_{eo}|\psi_e(\mathbf{k},i\omega)|^2|\psi_o(\mathbf{k},i\omega)|^2 + \frac{1}{2}g_{oe}|\psi_o(\mathbf{k},i\omega)|^2|\psi_e(\mathbf{k},i\omega)|^2. \end{aligned} \tag{D1}$$

Next, we expand the inverse local single-particle Green's function $G_{\sigma\sigma}^{-1}(i\omega)$ and dispersion $\epsilon_{\sigma\sigma'}(\mathbf{k})$ to quadratic order in $\mathbf{k}$ and ω, respectively, and we obtain

$$\begin{aligned} S_k = &\sum_{\mathbf{k},\omega} r_e\psi_e^*(\mathbf{k},i\omega)\psi_e(\mathbf{k},i\omega) + K_{e1}\psi_e^*(\mathbf{k},i\omega)(-i\omega)\psi_e(\mathbf{k},i\omega) + K_{e2}(i\omega)\psi_e^*(\mathbf{k},i\omega)(-i\omega)\psi_e(\mathbf{k},i\omega) \\ &+ r_o\psi_o^*(\mathbf{k},i\omega)\psi_o(\mathbf{k},i\omega) + K_{o1}\psi_o^*(\mathbf{k},i\omega)(-i\omega)\psi_o(\mathbf{k},i\omega) + K_{o2}(i\omega)\psi_o^*(\mathbf{k},i\omega)(-i\omega)\psi_o(\mathbf{k},i\omega) \\ &+ \psi_e^*(\mathbf{k},i\omega)(-4t)\psi_o(\mathbf{k},i\omega) + K_3(-i\mathbf{k})\psi_e^*(\mathbf{k},i\omega)(i\mathbf{k})\psi_o(\mathbf{k},i\omega) \\ &+ \psi_o^*(\mathbf{k},i\omega)(-4t)\psi_e(\mathbf{k},i\omega) + K_3(-i\mathbf{k})\psi_o^*(\mathbf{k},i\omega)(i\mathbf{k})\psi_e(\mathbf{k},i\omega) \\ &+ \frac{1}{2}g_{ee}|\psi_e(\mathbf{k},i\omega)|^4 + \frac{1}{2}g_{oo}|\psi_o(\mathbf{k},i\omega)|^4 \\ &+ \frac{1}{2}g_{eo}|\psi_e(\mathbf{k},i\omega)|^2|\psi_o(\mathbf{k},i\omega)|^2 + \frac{1}{2}g_{oe}|\psi_o(\mathbf{k},i\omega)|^2|\psi_e(\mathbf{k},i\omega)|^2, \end{aligned} \tag{D2}$$

where $r_e = -(\frac{\bar{n}_e+1}{\varepsilon_{\bar{n}_e,0}-\varepsilon_{\bar{n}_e+1,0}} - \frac{\bar{n}_e}{\varepsilon_{\bar{n}_e-1,0}-\varepsilon_{\bar{n}_e,0}})^{-1}$, $r_o = -(\frac{\bar{n}_o+1}{\varepsilon_{0,\bar{n}_o}-\varepsilon_{0,\bar{n}_o+1}} - \frac{\bar{n}_o}{\varepsilon_{0,\bar{n}_o-1}-\varepsilon_{0,\bar{n}_o}})^{-1}$, $K_{e1} = \frac{\mu_e^2-(\bar{n}_e^2+\bar{n}_e-1)U^2+2\mu_eU}{(\mu_e+U)^2}$, $K_{o1} = \frac{\mu_o^2-(\bar{n}_o^2+\bar{n}_o-1)U^2+2\mu_oU}{(\mu_o+U)^2}$, $K_{e2} = \frac{\bar{n}_e(\bar{n}_e+1)U^2}{(\mu_e+U)^3}$, $K_{o2} = \frac{\bar{n}_o(\bar{n}_o+1)U^2}{(\mu_o+U)^3}$, and $K_3 = 2ta^2$. Then, we can obtain the effective action Eq. (10) in the main text by transforming the action Eq. (D2) back to real space.

APPENDIX E: THE LOW-ENERGY EXCITATION

To investigate the low-energy excitation of the system in an analytical way, we solve the equation $\det[M(\mathbf{k}, i\omega)] = 0$ in the $E \to 0$ limit via the following relation:

$$\big(C_9k^4 + C_8k^2 + C_7\big)E^4 + \big(C_6k^4 + C_5k^2 + C_4\big)E^2 + \big(C_3k^4 + C_2k^2 + C_1\big) = 0, \tag{E1}$$

where the coefficients are defined as $C_1 = (4t)^4 - 2\times(4t)^2[D_1D_2 + D_3D_4] + [(D_1^2 - D_3^2)(D_2^2 - D_4^2)]$, $C_2 = -4\times(4t)^3K_3 + 4\times(4t)K_3[D_1D_2 + D_3D_4]$, $C_3 = 6\times(4t)^2K_3^2 - 2K_3^2[D_1D_2 + D_3D_4]$, $C_4 = 2\times(4t)^2[K_{e2}D_2 + K_{o2}D_1 - K_{e1}K_{o1}] - K_{e1}^2(D_2^2 - D_4^2) - K_{o1}^2(D_1^2 - D_3^2) - 2K_{e2}[D_1(D_2^2 - D_4^2)] - 2K_{o2}[D_2(D_1^2 - D_3^2)]$, $C_5 = -4\times(4t)K_3K_{e2}D_2 - 4\times(4t)K_3K_{o2}D_1 + 4\times(4t)K_3K_{e1}K_{o1}$, $C_6 = -2K_3^2K_{e1}K_{o1} + 2K_3^2K_{e2}D_2 + 2K_3^2K_{o2}D_1$, $C_7 = -2\times(4t)^2K_{e2}K_{o2} + K_{e1}^2K_{o1}^2 + 2K_{o1}^2K_{e2}D_1 + 2K_{e1}^2K_{o2}D_2 + 4K_{e2}K_{o2}D_1D_2 + K_{e2}^2(D_2^2 - D_4^2) + K_{o2}^2(D_1^2 - D_3^2)$, $C_8 = 4\times(4t)K_3K_{e2}K_{o2}$, and $C_9 = -2K_3^2K_{e2}K_{o2}$ with $D_1 = r_e + 2g_{ee}n_{s,e}$, $D_2 = r_o + 2g_{oo}n_{s,o}$, $D_3 = g_{ee}n_{s,e}$, $D_4 = g_{oo}n_{s,o}$. By analytically solving the above equation and expanding the energy dispersion to the quartic order of the momentum, the low-energy excitation (lowest positive branch) can be approximately determined in the long-wave limit as

$$E^+_{\text{Goldstone}} \simeq \sqrt{I_2}k + \sqrt{I_4}k^2, \tag{E2}$$

where $I_2 = \frac{C_1C_5}{C_4^2} - \frac{C_2}{C_4}$, $I_4 = -\frac{C_1C_5^2}{C_4^3} + \frac{C_2C_5+C_1C_6}{C_4^2} - \frac{C_3}{C_4}$.

[1] K. Huang, *Statistical Mechanics* (Wiley, New York, 1987).
[2] Y. Nambu, Phys. Rev. **117**, 648 (1960).
[3] J. Goldstone, Nuovo Cimento **19**, 154 (1961).
[4] H. B. Nielsen and S. Chadha, Nucl. Phys. B. **105**, 445 (1976).
[5] F. Bloch, Z. Phys. **61**, 206 (1930).
[6] A. V. Chubukov, S. Sachdev, and J. Ye, Phys. Rev. B **49**, 11919 (1994).
[7] D. Podolsky and S. Sachdev, Phys. Rev. B **86**, 054508 (2012).
[8] J. Ye and L. Jiang, Phys. Rev. Lett. **98**, 236802 (2007).

[9] P. T. Ernst, S. Götze, J. S. Krauser, K. Pyka, D. S. Lühmann, D. Pfannkuche, and K. Sengstock, Nat. Phys. **6**, 56 (2010).
[10] S. B. Papp, J. M. Pino, R. J. Wild, S. Ronen, C. E. Wieman, D. S. Jin, and E. A. Cornell, Phys. Rev. Lett. **101**, 135301 (2008).
[11] J. Steinhauer, R. Ozeri, N. Katz, and N. Davidson, Phys. Rev. Lett. **88**, 120407 (2002).
[12] J. Stenger, S. Inouye, A. P. Chikkatur, D. M. Stamper-Kurn, D. E. Pritchard, and W. Ketterle, Phys. Rev. Lett. **82**, 4569 (1999).
[13] D. M. Stamper-Kurn, A. P. Chikkatur, A. Görlitz, S. Inouye, S. Gupta, D. E. Pritchard, and W. Ketterle, Phys. Rev. Lett. **83**, 2876 (1999).
[14] M. Kozuma, L. Deng, E. W. Hagley, J. Wen, R. Lutwak, K. Helmerson, S. L. Rolston, and W. D. Phillips, Phys. Rev. Lett. **82**, 871 (1999).
[15] Y.-X. Yu, J. Ye, and W.-M. Liu, Sci. Rep. **3**, 3476 (2013).
[16] J.-S. Pan, W. V. Liu, and X.-J. Liu, Phys. Rev. Lett. **125**, 260402 (2020).
[17] M. Greiner, O. Mandel, T. Esslinger, T. W. Hänsch, and I. Bloch, Nature (London) **415**, 39 (2002).
[18] T. Stöferle, H. Moritz, C. Schori, M. Köhl, and T. Esslinger, Phys. Rev. Lett. **92**, 130403 (2004).
[19] S. Sachdev, *Quantum Phase Transitions* (Cambridge University Press, Cambridge, 2011).
[20] M. Endres, T. Fukuhara, D. Pekker, M. Cheneau, P. Schauß, C. Gross, E. Demler, S. Kuhr, and I. Bloch, Nature (London) **487**, 454 (2012).
[21] D. Pekker and C. M. Varma, Annu. Rev. Condens. Matter. Phys. **6**, 269 (2015).
[22] R. Landig, L. Hruby, N. Dogra, M. Landini, R. Mottl, T. Donner, and T. Esslinger, Nature (London) **532**, 476 (2016).
[23] J. Klinder, H. Keßler, M. R. Bakhtiari, M. Thorwart, and A. Hemmerich, Phys. Rev. Lett. **115**, 230403 (2015).
[24] N. Dogra, F. Brennecke, S. D. Huber, and T. Donner, Phys. Rev. A **94**, 023632 (2016).
[25] J. K. Freericks and H. Monien, Europhys. Lett. **26**, 545 (1994).
[26] J. K. Freericks and H. Monien, Phys. Rev. B **53**, 2691 (1996).
[27] K. Sengupta and N. Dupuis, Phys. Rev. A **71**, 033629 (2005).
[28] J. K. Freericks, H. R. Krishnamurthy, Y. Kato, N. Kawashima, and N. Trivedi, Phys. Rev. A **79**, 053631 (2009).
[29] M. Faccioli and L. Salasnich, Phys. Rev. A **99**, 023614 (2019).
[30] R. Sensarma, K. Sengupta, and S. Das Sarma, Phys. Rev. B **84**, 081101(R) (2011).
[31] S. Sinha and K. Sengupta, Europhys. Lett. **93**, 30005 (2011).
[32] T. Graß, K. Saha, K. Sengupta, and M. Lewenstein, Phys. Rev. A **84**, 053632 (2011).
[33] S. Mandal, K. Saha, and K. Sengupta, Phys. Rev. B **86**, 155101 (2012).
[34] S. Powell, R. Barnett, R. Sensarma, and S. Das Sarma, Phys. Rev. Lett. **104**, 255303 (2010).
[35] K. Saha, K. Sengupta, and K. Ray, Phys. Rev. B **82**, 205126 (2010).
[36] X. Li, E. Zhao, and W. V. Liu, Phys. Rev. A **83**, 063626 (2011).
[37] Y. Chen, Z. H. Yu, and H. Zhai, Phys. Rev. A **93**, 041601(R) (2016).
[38] K. Baumann, C. Guerlin, F. Brennecke, and T. Esslinger, Nature (London) **464**, 1301 (2010).
[39] M. P. A. Fisher, P. B. Weichman, G. Grinstein, and D. S. Fisher, Phys. Rev. B **40**, 546 (1989).
[40] M. Faccioli and L. Salasnich, Symmetry **10**, 80 (2018).
[41] S. Weinberg, *The Quantum Theory of Fields* (Cambridge University Press, Cambridge, 1995), p. 76.
[42] P. Pippan, H. G. Evertz, and M. Hohenadler, Phys. Rev. A **80**, 033612 (2009).
[43] D. Clément, N. Fabbri, L. Fallani, C. Fort, and M. Inguscio, J. Low Temp. Phys. **158**, 5 (2009).